CrystEngComm

Accepted Manuscript

ROYAL SOCIETY OF CHEMISTRY

www.rsc.org/crystengcomm

The Structural Diversity and Properties of Nine New Viologen based Zwitterionic Metal-Organic Frameworks

Darpandeep Aulakh, Anthony P. Nicoletta, Juby R. Varghese and Mario Wriedt*

Department of Chemistry & Biomolecular Science

Clarkson University

8 Clarkson Ave

Potsdam, NY 13699

United States of America

* Tel.: +1 (315) 268-2355

Fax: +1 (315) 268-6610

Email: mwriedt@clarkson.edu

Abstract

The neutral flexible viologen based ligand 1,1'-bis(4-carboxybenzyl)-4,4'-bipyridinium dibromide (H_2**L**Br_2) and its self-assembly with first-row transition metals in an aqueous media leads to the formation of nine new zwitterionic (ZW) MOF materials with the following compositions: $\{[CuBr(L)]\cdot(OH)\cdot 7H_2O\}_n$ (**1**); $\{[M_4(L)_6(OH_2)_{12}]\cdot 2Br\cdot 3(bdc)\cdot 33H_2O\}_n$ with M = Mn (**2**), Co (**3**) and Ni (**4**), $\{[M(bdc)(L)_{1.5}]\cdot 9H_2O\}_n$ with M = Cd (**5**) and Zn (**6**); $\{[Cu_2(3\text{-}pzc)_2(L)(OH_2)]\cdot 5H_2O\}_n$ (**7**); $\{[ZnCl_2(L)_{0.5}]\cdot 0.33H_2O\}_n$ (**8**) and $[Pd(HL)(Br)_2(NO_2)_2(OH_2)_2]$ (**9**) (bdc = 1,4-benzenedicarboxylate, pzc = 3-pyrazole carboxylate). These compounds were characterized by single-crystal X-ray diffraction (SCXRD), powder X-ray diffraction (PXRD), infrared spectrometry (IR), elemental analyses, thermogravimetric analyses (TGA) and differential scanning calorimetry (DSC). Interestingly, when the samples are exposed to UV irradiation, photochromic behavior is observed for the ligand only, whereas the ZW MOFs are found to be photochemically inert. The fundamental structural origin for this photo reactivity is discussed in detail, as well as an in-depth CSD analysis of important intra- and intermolecular parameters of **L**-based MOFs.

Introduction

Since the beginning of the 20th century, metal-organic frameworks (MOFs) have emerged as promising materials for applications in heterogeneous catalysis,[1-4] molecular recognition and separation,[5-8] gas storage,[9-13] sensing[14-16] and ion exchange.[17-19] These are inorganic-organic hybrid materials constructed from metal ions or clusters and bridged by polytypic organic linkers to build one-, two-, or three-dimensional infinite networks. The structure and functionality of these hybrids significantly depends on the selection of the metallic nodes and the bridging organic linkers, as well as the type of connection between the two. Given the ex-

traordinary degree of variability in both the organic and inorganic components of these structures, adjusting the variables allows for selective tailoring of the framework structures, pore environment and functionalities.[20-26] In particular, the conformational mobility around flexible bridging organic linkers results in various versatile conformations, providing the means to generate structural diversity, and thus allowing for the control of MOF architectures.

Recently, a new class of MOF materials, namely zwitterionic (ZW) MOFs, have exhibited interesting adsorption,[11, 27, 28] luminescent,[29] magnetic[30-34] and photochromic[35-38] behaviors. These properties are due to the uniquely charged organic surfaces (COSs) embedded in their structures. Generated through positively charged pyridinium units and negatively charged carboxylate units within ZW ligands, COSs can be systematically tuned by the variation of intramolecular pyridinium-carboxylate distances and their relative flexible intramolecular orientation. In this context we report a new design strategy to access ZW MOFs from anionic viologen derivates.[39] With this approach we show that the anionic ZW ligand 1,1'-bis(3,5-dicarboxybenzyl)-4,4'-bipyridinium dibromide can be used to rationally design new ZW MOFs which do not require additional counter ions for charge compensation of a charged-balanced neutral MOF. Intrigued by these outcomes, we proceeded to systematically investigate the structural diversity of ZW MOFs constructed from the viologen derivate 1,1'-bis(4-carboxybenzyl)-4,4'-bipyridinium dibromide (H_2**L**Br_2).

Upon deprotonation, this ligand is considered a neutral ZW ligand, and thus counter anions such as halides (Cl^-, Br^-), 1,4-benzenedicarboxylate (bdc^{2-}) and 3-pyrazole carboxylate (pzc^{2-}) were employed in the MOF synthesis, counterbalancing the positively charged metal centers. Please note, that monodentate halides are usually incorporated as terminal ligands in MOF frameworks, whereas bdc^{2-} and pzc^{2-} being polydentate ligands are mostly found to be co-ligands of bridging nature. The methylene groups in **L** link the pyridinium and phenyl units which deviate the whole ligand from linearity and impart flexibility to the molecular

framework. The linear distance of ~21.5 Å between the terminal carboxylate groups in the ligand and its ditopic nature makes it suitable for the synthesis of extended coordination networks and macrocycles.

Within the past 10 years a few **L**-based compounds have been reported,[27, 28, 31, 35-38, 40-43] including a series of three isostructural transition metal coordination polymers reported by Yang *et al.*[40]. These 2-D non-interpenetrating frameworks exhibited large honeycomb-like hexagonal cavities and were stabilized by the steric hindrance of the ligand's backbone between the frames and by the hydrogen bonding interactions. An interpenetrated diamondoid network coordination polymer with a hexa-coordinated Cu(II) paddlewheel dimer as a connecting node, reported by Zhang *et al*.,[31] exhibited interesting electronic transition and magnetic properties. Another study, revealed how a photochemically inert framework can be modified to become photosensitive through variation of temperature and the post-synthetic exchange of anions in a single crystal-to-single crystal fashion.[27] Furthermore, Zhang *et al.*[38] reported on the photochromic behavior of coordination network $\{[Cd(bdc)(L)_{1.5}]\cdot 10H_2O\}_n$ in which the flexible conformation of the bipyridinium unit leads to a sandwich-type donor-acceptor-donor stacking, facilitating the photoinduced and thermal-induced reduction of the bipyridinium ligand.

In the herein presented fundamental study we report the systematic investigation of the synthesis and structural characterization of nine new ZW MOF materials with **L** as the fundamental building block. We demonstrate that the crystal structures can be significantly modified as a result of, (a) the incorporation of different anionic counterions and (b) the flexibility of the bipyridinium moieties.

Experimental

General Information

Commercially available reagents were used as received without further purification. The ZW ligand 1,1'-bis(4-carboxybenzyl)-4,4'-bipyridinium dibromide (H_2**L**Br_2) was synthesized with enhanced product yield by employing a slightly modified procedure as reported previously by Sun *et al.*[40] (see below).

Synthesis of the 1,1'-bis(4-carboxybenzyl)-4,4'-bipyridinium dibromide (H_2L**Br_2)**

4,4'-bipyridine (1.56 g, 10 mmol) and 3 equivalents of 4-carboxybenzyl bromide were dissolved in 20 mL of acetonitrile and refluxed for 24 hours at 100 °C. After the mixture was cooled to room temperature, the resulting precipitates were filtered off, washed with acetonitrile and dried in vacuum to give H_2**L**Br_2 as light green powder (6.66 g, yield 78%). ^{1}H-NMR (400 MHz, D_2O): δ = 9.24 (*d*, 2H); 8.55 (*d*, 2H); 8.09 (*d*, 2H); 7.58 (*d*, 2H); 6.01 (*s*, 2H) (Figure S1). IR (KBr pellet, cm^{-1}): $\tilde{\nu}$ = 3419 (w), 3119 (s), 3075 (s), 2999 (s), 2589 (s), 2435 (s), 1696 (s), 1636 (s), 1578 (s), 1559 (m), 1511 (s), 1453 (s), 1420 (m), 1385 (m), 1313 (m), 1220 (m), 1188 (s), 1117 (s), 1019 (w), 860(s), 811 (s), 782 (w), 744 (s), 703 (s), 591 (s), 466 (s) (Figure S2).

Various attempts to grow single crystals of **L** were not successful. However, the following procedure coincidentally resulted in single crystals of composition (H_2**L**$)_2 \cdot SO_4 \cdot HSO_4 \cdot Br \cdot 2H_2O$: H_2**L**Br_2 (29.31 mg, 0.05 mmol) was dissolved in 1 mL of water and the pH was adjusted to 7 with 0.1 mol L^{-1} NaOH. A mixture of $Zr(SO_4)_2 \cdot 4H_2O$ (35.5 mg, 0.1 mmol) and 1,4-benzene dicarboxylic acid (16.6 mg, 0.1 mmol) in 1 mL of water was added to this solution. The resulting mixture was stirred in a closed glass vial on a heating plate at 70 °C for 30 minutes and filtered off. The filtrate was allowed to stand for several weeks at room temperature to give ivory colored plate shaped single crystals.

Synthesis of {[CuBr(L)]·(OH)·7H_2O}$_n$ (1)

Bulk material preparation: H_2**L**Br_2 (29.3 mg, 0.05 mmol) was dissolved in 1 mL of water and pH was adjusted to 7 with 0.1 mol L^{-1} NaOH. A mixture of $Cu(CH_3COO)_2$ (90.8 mg, 0.5

mmol) and 1,4-benzene dicarboxylic acid (16.6 mg, 0.1 mmol) in 1 mL of water was added to this solution. Clear blue colored polycrystalline precipitate was obtained after stirring the mixture in a closed glass vial on a heating plate at 85 °C for 12 hours. The residue was filtered off and washed with water and diethyl ether and dried in air. The filtrate was set aside to grow single crystals (see below). The purity of the bulk material was confirmed by X-ray powder diffraction (Figure S3). Although benzene dicarboxylic acid is not incorporated in the structure of **1**, we found that **1** could not be obtained in its absence. Yield 42% based on the ligand. Calculated for $C_{26}H_{35}BrCuN_2O_{12}$ (711.01): C 43.92, H 4.01, N 3.94; found: C 43.94, H 3.71, N 3.82. IR (KBr pellet, cm^{-1}): $\tilde{\nu}$ = 3423 (w), 3120 (s), 3037 (w), 2870 (s), 1635 (m), 1569 (m), 1559 (m), 1442 (s), 1404 (s), 1315 (m), 1191 (s), 1017 (s), 854 (s), 794 (s), 771 (s), 702 (m), 594 (s), 509 (s) (Figure S2).

Single crystals suitable for X-ray structure determination were prepared in a similar fashion as described above, but the filtrate obtained in the last step was allowed to stand for several days at room temperature to give clear blue block-shaped single crystals.

$\{[M_4(L)_6(OH_2)_{12}]\cdot 2Br\cdot 3(bdc)\cdot 33H_2O\}_n$ [M = Mn (2), Co (3) and Ni (4)]

Bulk materials and single crystals were prepared similarly to 1, but instead of using $Cu(CH_3COO)_2$, $Mn(CH_3COO)_2\cdot 4H_2O$ (0.5 mmol, 122.5 mg) was used for **2,** $Co(CH_3COO)_2\cdot 4H_2O$ (0.5 mmol, 124.5 mg) for **3**, and $Ni(CH_3COO)_2$ (0.5 mmol, 88.4 mg) for **4**. The purity of the bulk materials were confirmed by X-ray powder diffraction (Figure S4). Yield for **2**: 72% based on **L**, for **3**: 68% based on **L**, for **4**: 65% based on **L**. Calculated for **2**: $C_{180}H_{210}Br_2Mn_4N_{12}O_{81}$ (4223.20): C 51.19, H 5.15, N 3.98; found: C 50.73, H 5.03, N 4.02, for **3**: $C_{180}H_{198}Br_2Co_4N_{12}O_{75}$ (4125.07): C 52.41, H 4.84, N 4.07; found: C 51.45, H 4.68, N 4.01, for **4**: $C_{180}H_{210}Br_2Ni_4N_{12}O_{81}$ (4232.20): C 51.08, H 5.00, N 3.97; found: C 48.17, H 5.00, N 3.93. IR (KBr pellet, cm^{-1}) for **2**: $\tilde{\nu}$ = 3423 (w), 3119 (m), 3060 (w), 2666 (w), 1635 (s), 1573 (s), 1555 (m), 1421 (s), 1388 (w), 1287 (s), 1019 (s), 859 (s), 798 (m), 769 (m), 702

(m), 596 (s), 511 (s), for **3**: $\tilde{\nu}$ = 3422 (w), 3120 (m), 3060 (w), 2667 (w), 1635 (s), 1575 (s), 1556 (m), 1422 (s), 1381 (w), 1287 (s), 1019 (s), 849 (s), 799 (m), 769 (m), 704 (m), 593 (s), 527 (s), for **4**: $\tilde{\nu}$ = 3416 (w), 3120 (m), 3052 (w), 1637 (s), 1597 (s), 1557 (m), 1447 (s), 1374 (w), 1281 (s), 1016 (s), 860 (s), 807 (m), 768 (m), 708 (m), 596 (s), 512 (s) (Figure S2).

Synthesis of $\{[M(bdc)(L)_{1.5}]\cdot 9H_2O\}_n$ [M = Cd (5) and Zn (6)]

Single crystals were prepared as described for **1**, except instead of using $Cu(CH_3COO)_2$, $Cd(CH_3COO)_2\cdot 2H_2O$ (0.5 mmol, 133.3 mg) was used for **5,** and $Zn(CH_3COO)_2\cdot 2H_2O$ (0.5 mmol, 109.8 mg) for **6**. No phase pure bulk material could be synthesized; crystals were grown in a heterogeneous mixture of unknown byproducts which could not be separated.

Synthesis of $\{[Cu_2(3\text{-}pzc)_2(L)(OH_2)]\cdot 5H_2O\}_n$ (7)

Single crystals were prepared as described for **1**, except instead of using 1,4-benzene dicarboxylic acid, pyrazole-3-carboxylic acid (0.05mmol, 5.6 mg) was used. No phase pure bulk material could be synthesized; crystals were grown in a heterogeneous mixture of unknown byproducts which could not be separated.

Synthesis of $\{[ZnCl_2(L)_{0.5}]\cdot 0.33H_2O\}_n$ (8)

Single crystals were prepared with the following procedure: H_2**L**Br_2 (29.31 mg, 0.05 mmol) was dissolved in 1 mL of water and the pH was adjusted to 7 with 0.1 mol L^{-1} NaOH. A solution of $ZnCl_2$ (0.1 mmol, 13.62 mgs) in 1 mL of 1,2-dimethoxyethane was added and the resulting mixture was heated in a closed glass vial at 120 °C without stirring for three days. On cooling, clear white plate-shaped crystals were obtained as a major phase. No phase pure bulk material could be synthesized; crystals were grown in a heterogeneous mixture of unknown byproducts which could not be separated.

Synthesis of $[Pd(HL)(Br)_2(NO_2)_2(OH_2)_2]$ (9)

Single crystals were prepared with the following procedure: H_2**L**Br_2 (58.62 mg, 0.1 mmol) was dissolved in 1 mL of water and the pH was adjusted to 7 with 0.1 mol L^{-1} NaOH.

$Pd(NO_3)_2$ (11.5 mg, 0.05 mmol) dissolved in 1 mL of water was added to the solution. The resulting mixture was stirred in a closed glass vial on a heating plate at 70 °C for 30 minutes and filtered off. The filtrate was allowed to stand for several weeks at room temperature resulting in needle shaped single crystals. No phase pure bulk material could be synthesized; crystals were grown in a heterogeneous mixture of unknown byproducts which could not be separated.

Single-Crystal Structure Analysis

Data collections were performed on single crystals coated with Paratone-N oil and mounted on Kapton loops. Single crystal X-ray data of all compounds were collected on a Bruker Kappa Apex II X-ray diffractometer outfitted with a Mo X-ray source (sealed tube, λ = 0.71073 Å) and an APEX II CCD detector equipped with an Oxford Cryosystems Desktop Cooler low temperature device. The APEX-II software suite was used for data collection, cell refinement, and reduction.[44] Absorption corrections were applied using SADABS[45]. Space group assignments were determined by examination of systematic absences, *E*-statistics, and successive refinement of the structures. Structure solutions were performed with direct methods using SHELXT-2014, and refined by least-squares refinement against $|F|^2$ followed by difference Fourier synthesis using SHELXL-2014.[46-48] All non-hydrogen atoms were refined with anisotropic displacement parameters. If not stated differently the O-H-hydrogen atoms were located in the difference map, where the bond lengths were set to ideal values with $d_{O\text{-}H}$ = 0.84 Å and refined using a riding model. The C-H atoms were positioned with idealized geometry and were refined with fixed isotropic displacement parameters [$U_{eq}(H) = -1.2 \cdot U_{eq}(C)$] using a riding model with $d_{C\text{-}H}$ = 0.95 Å (aromatic) and 0.99 Å (methylene).

In $(H_2L)_2 \cdot SO_4 \cdot HSO_4 \cdot Br \cdot 2H_2O$, H14 is disordered over two positions with site occupancy factors (SOFs) of 1/2 imposed by its location around a center of inversion, and thus, the resulting SO_4-HSO_4 dimer features an almost symmetrical H bonding between the SO_4^{2-} and

HSO_4^- anion. In **1**, no reasonable structural model could be found for some non-coordinating fragments and thus, the data were corrected using the solvent mask option in OLEX2.[49] MASK estimated a total count of 584.0 electrons per 1394.5 $Å^3$ of solvent accessible volume in **1**, which is in rough agreement to be seven water molecules and one hydroxide anion (Z = 8; H_2O = 10 e^-; OH^- = 9 e^-; 584.0 $e^-/8$ = 73 e^- ≈ 7 H_2O + 1 OH^-). In **2**, **3** and **4**, the bromide anion is disordered over three positions (Br1, Br2 and Br3) with SOFs of 1/3, 1/6 and 1/6 respectively. In addition, the following non-coordinating water molecules are disordered over two positions: O7W/O7W' (SOFs 2/5, 3/5) and O8W/O8W' (SOFs 1/4, 3/4) in **2**; O5W/O5W' (SOFs 1/4, 3/4), O6W/O6W' (SOFs 1/2, 1/2) and O7W/O7W' (SOFs 1/5, 4/5) in **3**; O6W/O6W' (SOFs 1/2, 1/2) and O7W/O7W' (SOFs 1/4, 3/4) in **4**. No reasonable anisotropic displacement parameters were found for the following non-coordinating atoms and thus, they were refined isotropically: O5W, O6W and O7W/O7W' in **2**; O6W/O6W' and Br3 in **3**; O5W, O6W/O6W', O7W/O7W' and Br2/Br3 in **4**; and O7W in **7**. H atoms were not located in the electron density map for all disordered and isotropically refined water molecules. Details of the structure determination are given in Table 1 and comments on B-alerts of checkcif reports are given in the SI.

CCDC-1441122-1441131 contains the supplementary crystallographic data for this manuscript. These data can be obtained free of charge from the Cambridge Crystallographic Data Centre via www.ccdc.cam.ac.uk.

Table 1. Selected crystal data and details on the structure determinations from single crystal data for the ligand H_2**L** and compounds **1-9**.

Compound	**H_2L**	**1**	**2**	**3**	**4**
Formula	$S_2C_{52}H_{50}N_4O_{18}$	$CuC_{26}H_{20}BrN_2O_4$	$Mn_4C_{180}H_{198}Br_2N_{12}O_{81}$	$Co_4C_{180}H_{204}Br_2N_{12}O_{81}$	$Ni_4C_{180}H_{204}Br_2N_{12}O_{81}$
MW [g·mol^{-1}]	1168.99	567.89	4202.07	4227.08	4226.20
Crystal system	Monoclinic	Tetragonal	Trigonal	Trigonal	Trigonal
Space group	$P2_1/n$	I-42d	R-3	R-3	R-3
a [Å]	12.4860(1)	13.2570(5)	34.9259(6)	35.0155(8)	35.0383(2)
b [Å]	14.7786(1)	13.2570(5)	34.9259(6)	35.0155(8)	35.038
c [Å]	13.7673(1)	31.1199(1)	27.7797(6)	27.5842(7)	27.5613(1)
α [deg]	90	90	90	90	90
β [deg]	104.077(3)	90	90	90	90
γ [deg]	90	90	120	120	120
V [Å^3]	2464.1(3)	5469.3(5)	29346.3(12)	29289.5(15)	29304(3)
T [K]	170(2)	170(2)	170(2)	170(2)	170(2)
Z	2	8	6	6	6
D_{calc} [g·cm^{-3}]	1.567	1.379	1.428	1.438	1.437
μ [mm^{-1}]	1.003	2.291	0.759	0.829	0.887
Min/max transmission	0.826/0.899	0.670/0.772	0.895/0.922	0.872/0.931	0.853/0.885
θ_{max} [deg]	28.383	28.529	28.293	28.308	28.286
Measured reflections	38298	27303	99516	89750	81866
Unique reflections	6127	3469	16211	16166	16175
Reflections [$F_0 > 4\sigma(F_0)$]	4444	2227	10152	11508	6702
Parameter	352	155	864	875	853
R_{int}	0.0476	0.0558	0.0647	0.0532	0.0598
R_1 [$F_0 > 4\sigma(F_0)$]	0.0386	0.0591	0.0615	0.0492	0.0645
wR_2 [all data]	0.1009	0.1887	0.1890	0.1436	0.1942
GOF	1.013	1.025	1.029	1.020	1.033
$\Delta\rho_{max}/\Delta\rho_{min}$ [e·Å^{-3}]	0.892/-0.627	1.050/-0.553	1.130/-0.644	0.926/-0.721	1.962/-0.945

Compound	**5**	**6**	**7**	**8**	**9**
Formula	$CdC_{47}H_{52}N_3O_{19}$	$ZnC_{47}H_{52}N_3O_{19}$	$Cu_2C_{34}H_{36}N_6O_{14}$	$ZnC_{13}H_{10}Cl_2NO_{2.17}$	$PdC_{26}H_{26}Br_2N_4O_{10}$
MW [g·mol^{-1}]	1075.31	1028.28	895.77	351.15	820.73
Crystal system	Monoclinic	Monoclinic	Monoclinic	Monoclinic	Triclinic
Space group	$P2_1/c$	$P2_1/c$	$P2_1/c$	$C2/c$	P-1
a [Å]	12.1281(2)	12.4870(6)	11.9508(2)	12.7183(4)	8.1476(2)
b [Å]	16.5109(3)	16.0350(8)	17.898(2)	14.0183(5)	8.2521(2)
c [Å]	23.7085(5)	23.5332(1)	16.975(2)	16.7134(6)	12.398(3)
α [deg]	90	90	90	90	80.843(8)
β [deg]	93.5049(1)	94.8080(17)	93.774(5)	110.7756(18)	72.380(7)
γ [deg]	90	90	90	90	67.642(7)
V [Å^3]	4738.65(15)	4695.4(4)	3623.0(8)	2786.06(17)	733.8(3)
T [K]	170(2)	170(2)	170(2)	170(2)	170(2)
Z	4	4	4	8	1
D_{calc} [g·cm^{-3}]	1.507	1.455	1.642	1.674	1.857
μ [mm^{-1}]	0.543	0.606	1.256	2.143	3.418
Min/max transmission	0.906/0.950	0.892/0.926	0.865/0.799	0.700/0.824	0.465/0.599
θ_{max} [deg]	28.332	28.323	25.350	28.259	28.362
Measured reflections	89372	65679	43330	25073	9915
Unique reflections	11725	11676	6643	3451	3495
Reflections [$F_0 > 4\sigma(F_0)$]	7824	5390	3510	2628	1970
Parameter	658	634	522	177	197
R_{int}	0.0880	0.1546	0.1753	0.0375	0.0687
R_1 [$F_0 > 4\sigma(F_0)$]	0.0439	0.0677	0.0900	0.0507	0.0484
wR_2 [all data]	0.1123	0.1848	0.2320	0.1778	0.1058
GOF	1.000	0.985	1.029	1.062	0.989
$\Delta\rho_{max}/\Delta\rho_{min}$ [e·Å^{-3}]	0.927/-0.721	0.885/-0.717	1.879/-0.907	1.406/-0.807	0.837/-0.769

Elemental Analysis

Elemental analyses (C, H, and N) were completed by Atlantic Microlab, Inc.

Powder X-Ray Diffraction (PXRD)

Powder X-ray diffraction patterns were recorded on a Bruker D2 Phaser diffractometer equipped with a Cu sealed tube (λ = 1.54178 Å). Powder samples were dispersed on low-background discs for analyses. Simulations of the PXRD data were performed by using single crystal data and the Powder Pattern module of the Mercury CSD software package.[50]

Spectroscopy

FT-IR data were recorded on a Nicolet iS10 from Thermo Scientific. ^{1}H-NMR data were recorded on Avance DMX-400 from Bruker.

Thermogravimetric Analysis (TGA)

TG data were recorded using a TGA Q50 from TA Instruments. All measurements were performed using platinum crucibles in a dynamic nitrogen atmosphere (50 mL/min) and a heating rate of 3 °C·min^{-1}. The instrument was corrected for buoyancy and current effects, and was calibrated using standard reference materials.

Differential Scanning Calorimetry (DSC)

DSC data were recorded using a TGA Q20 from TA Instruments. All measurements were performed using T zero aluminum pans, a dynamic nitrogen atmosphere (50 mL/min) and a heating rate of 3 °C·min^{-1}. The instrument was calibrated using standard reference materials.

Results and Discussion

Crystal structure of $(H_2L)_2 \cdot SO_4 \cdot HSO_4 \cdot Br \cdot 2H_2O$

The ligand crystallizes in the monoclinic space group $P2_1/n$ with the asymmetric unit consisting of one molecule of the protonated ligand H_2**L**, and one water molecule, both located on general positions; one half-occupied bromide anion located on a center of inversion, and one

half-occupied $SO4^{2-}$ anion superimposed on one half-occupied HSO_4^- anion. Symmetry growth shows that its H atom is disordered around a center of inversion resulting in the formation of an almost symmetrical H bond bridging these anions into a SO_4-HSO_4 dimer (Figure 1). The pyridinium rings of the viologen unit of **L** are almost co-planar with a dihedral angle of 3.06(1)°, and their 4-carboylbenzyl units are roughly perpendicular to the viologen motif with dihedral angles of 73.29(1)/74.95(1)°, while being aligned almost parallel to each other with a dihedral angle of 1.14(1)°. The methylene groups used as knots to link together the pyridinium and the 4-carboxylphenyl units impart flexibility to the ligand, which in turn results in a zig-zag conformation (Figure 1).

Figure 1. Crystal structure for $(H_2L)_2{\cdot}SO_4{\cdot}HSO_4{\cdot}Br{\cdot}2H_2O$ with displacement ellipsoids drawn at the 50% probability level. Selected atoms are labelled, symmetry code: A = -x + 3, -y + 1, -z - 2.

Crystal structure of $\{[CuBr(L)]\cdot(OH)\cdot 7H_2O\}_n$ (1)

Compound **1** crystallizes in the non-centrosymmetric tetragonal space group *I*-42*d* with eight formula units. The asymmetric unit consists of one half occupied copper(II) cation, one bromide anion and a half ligand molecule. In the crystal structure each Cu(II) cation is pentacoordinated by one bromide ion and one pair of two symmetry equivalent carboxylate oxygen atoms of **L** (Figure 2A). Bridging ligands form the common paddlewheel dimeric unit of composition $[Cu_2(CO_2)_4(Br)_2]$ resulting in a three-dimensional polymeric framework, with the bromide anions located in the axial positions of the paddlewheel. The pyridinium rings of the 4,4′-bipyridinium unit of **L** are slightly twisted with a dihedral angle of 29.67(3)°, while the 4-carboxybenzyl units are significantly twisted from the respective neighboring pyridinium rings with dihedral angles of 71.22(4)° and 84.41(4)° (Figure 2B). This results in the devia-

tion from linearity of **L** which thereby exhibits a zig-zag conformation. Because of the length and flexibility exhibited by **L**, the metal cations in the framework do not lie in the same plane as **L**, as evident from views of the packing structure along the crystallographic *b* and *c* axes (Figure 2C, D). Overall, owing to (a) the distance of 18.25(5) Å between two $[Cu_2(CO_2)(Br_2)]$ motifs, which results in large cavities, and (b) the structural flexibility exhibited by **L**, an unusual 9-fold interpenetration in the framework or three sets of normal three fold nets can be found in the crystal structure of **1** (Figure 2E), as described in detail for the isostructural compound $\{[Cu_2(L)_2(NO_3)_2]\cdot 0.5Cl\cdot 0.5(OH)\cdot(NO_3)\cdot H_2O\}_n$ reported by Zhang *et al.*[31]

Figure 2. (A) Crystal structure of **1** with view on the coordination sphere of the Cu(II) cation with displacement ellipsoids drawn at the 50% probability level. Selected atoms are labelled. Symmetry codes: A = -x - 3, y, -z, B = x, -y - 3, -z and C = -x - 3, -y - 3, z; (B) structural conformation of **L** in **1** with view along the *b* axis; (C) side view of an independent network of **1** along the *b* axis and (D) along the *c* axis in the space-filling mode; and (E) interpenetrated framework of **1** with view along the *a*-axis, hydrogen atoms are removed for the sake of clarity.

Crystal structures of $\{[M_4(L)_6(OH_2)_{12}]\cdot 2Br\cdot 3(bdc)\cdot 33H_2O\}_n$ [M = Mn (2), Co (3) and Ni (4)]

Compounds **2-4** crystallize in the tetragonal space group *R*-3 and are isostructural to $\{[M_2(L)_3(OH_2)_6]\cdot 4(OH)\cdot 15H_2O\}_n$ [M = Mn, Co, Ni], reported by Yang *et al.*[40] and $\{[Mn_4(L)_6(OH_2)_{12}]\cdot 3(bdc)\cdot 3(OH)\cdot 30H_2O\}_n$ by Zhang *et al.*[28] with the difference being that in compounds **2-4** bromide anions and/or bdc co-ligands (bdc = 1,4-benzenedicarboxylate) were employed as counterions to balance the M(II) cations. Each asymmetric unit consists of one full and one 1/3 occupied M(II) cation, two metal-coordinating **L**, one non-coordinating bdc

co-ligand, four coordinating and eleven non-coordinating water molecules and one 2/3 occupied bromide ion disordered over three positions (site occupation factors: 1/3, 1/6, 1/6). In the crystal structure each M(II) cation is coordinated by three carboxylate oxygen atoms from three **L** ligands and three water molecules in a distorted octahedral geometry, resulting in a MO_6 octahedron that exhibits M-O_L bond distances in the range of 2.032(1)-2.115(1) Å for **2,** 2.076(0)-2.137(2) Å for **3** and 2.059(1)-2.090(2) Å for **4**; and M-O_{water} distances in the range of 2.192(1)-2.231(1) for **2**, 2.089(0)-2.136(2) Å for **3** and 2.059(2)-2.096(2) Å for **4** (Figure 3A; and SI Figures S5, S6). The voids created by **L** and the metal centers are occupied by the bdc co-ligands along with the non-coordinating water molecules and the bromide anion.

Figure 3. (A) Crystal structure of **3** as a representative example for **2** and **4** with view of the coordination sphere of the Co(II) cation with displacement ellipsoids drawn at the 30% probability level. Selected atoms are labelled. Symmetry codes: A = 0.66 + x – y, 0.33 + x, 1.33 – z; B = -y +2, x – y + 2, z; C = -x + y, -x + 2, z. For Ortep plots of **2** and **4** see figures S5 and S6 in the SI; (B) structural conformation of **L** in **3** along the *c* axis; (C) side view of an independent network of **3** along the *b* axis and (D) along the *c* axis in the space-filling mode; and (E) crystal packing of **3** along the *a* axis. Hydrogen atoms, disordered bromide ions, bdc ligands and non-coordinating water molecules are removed for the sake of clarity.

Each **L** ligand bridges two metal cations through two carboxylate groups in a monodentate chelation mode (Figure 3A). The pyridinium rings of the 4,4′-bipyridinium unit of **L** are slightly twisted with dihedral angles of 6.12(1)°, 6.01(2)° and 5.86(1)° in **2**, **3** and **4** respectively, while the 4-carboxylbenzyl units are significantly twisted from the neighboring pyridinium rings with dihedral angles of 69.69(1)/72.21(1)°, 72.87(2)/76.46(1)°, 87.61(2)/77.43(3)° in **2**, **3** and **4** respectively; and the two 4-carboxybenzyl units are aligned

roughly parallel to each other with dihedral angles of 5.49(1)° in **2**, 9.35(2)° in **3** and 5.43(1)° in **4**. As a result, the whole ligand is not linear and hence exhibits a zig-zag conformation (Figure 3C, D). The M(II) centers serve as 3-connected nodes in the framework, thereby creating an infinite 2-D network, which contains large edge-sharing hexagons with a metal cation at each corner and a **L** molecule at each edge (Figure 3D). The two 4-carboxylbenzyl units of each **L** are parallel to each other and lie "above" and "below" the hexagonal grids alternately. Extended interlayer hydrogen bonding interactions among water molecules and non-coordinating carboxylate oxygen atoms of **L** lead to the formation of a 3-D supramolecular network **(**Figure 3E).

Crystal structures of $\{[M(L)_{1.5}(bdc)]\cdot 9H_2O\}_n$ [M = Cd (5) and Zn (6)]

Compounds **5** and **6** crystallize in the monoclinic space group $P2_1/c$ with each asymmetric unit consisting of one M(II) cation coordinated to one and a half molecule of **L**, one metal-coordinating bdc co-ligand and nine non-coordinating water molecules. In the crystal structure each M(II) cation is coordinated to seven O atoms, two from one carboxylate of the bdc co-ligand and five from the carboxylate groups of three symmetry related **L**, giving rise to a distorted capped trigonal prism with M-$O_{\mathbf{L}}$ distances ranging from 2.183(1)-2.742(2) Å in **5** and 1.954(2)-2.690(1) Å in **6** (Figure 4A). Different conformations and coordination modes are exhibited by **L** owing to its flexible nature. **L** imparts *trans* and *cis* orientations in the crystal structure where $\mathbf{L}_{trans}$ adopts a *bis*-bidentate coordination mode, while the $\mathbf{L}_{cis}$ exhibits bidentate chelation on one end and monodentate on the other (Figure 4B). A macrocyclic ring $[M_2(\mathbf{L}_2)]$ is formed by the coordination of **L** to the metal centers in *cis* conformation and connected to another ring through **L** in *trans* conformation to form 1-D chains (Figure 4C), which are entangled in pairs to give rise to polyrotaxanes. The bdc co-ligands coordinate in monobidentate fashion and act like open arms dangling from both sides of the chains into the mac-

rocyclic ring (Figure 4C). The polyrotaxane layers are further mutually polythreaded by lateral arms into 3-D polypseudorotoxane arrays, which are discussed in detail by Zhang *et al.*[38] for the isostructural material $\{[Cd(L)_{1.5}(bdc)]\cdot 10H_2O\}_n$ (Figure 4D).

Figure 4. (A) Crystal structure of **5** with view on the coordination sphere of the Cd(II) cation with displacement ellipsoids drawn at the 50% probability level. Selected atoms are labelled. Symmetry codes: A = -x + 1, -y - 2, -z, B = -x - 1, -y - 1, -z + 1; for ortep plot of **6** see figure S7 in the SI; (B) structural conformation of **L** in **5** along the *b* axis, bdc units coordinating to the metal centers have been removed for the sake of clarity; (C) view along the *b* axis of an independent 1-D chain of **5** with bdc units; (D) perspective view of an independent polyrotaxane sheet along the *a* axis; hydrogen atom are not shown for the sake of clarity.

Crystal structure of $\{[Cu_2(L)(pzc)_2(OH_2)]\cdot 6H_2O\}_n$ (7)

Compound **7** crystallizes in the monoclinic space group $P2_1/c$ with the asymmetric unit consisting of two Cu(II) cations, one **L** molecule and two pzc co-ligands (pzc = 3-pyrazole carboxylate), one metal-coordinating and six non-coordinating water molecules with all the atoms in crystallographically independent general positions. In the crystal structure Cu1 is coordinated by one **L** and two pzc co-ligands, and one water molecule in a distorted octahedral geometry, while Cu2 is coordinated in a similar fashion, except that the water molecule is replaced by a carboxylate O atom of a symmetry equivalent pzc co-ligand. A $[Cu_2(pzc)_2]$ dimer is formed by each pzc ligand linking two metal cations through one carboxylate O atom and two adjacent nitrogen atoms in a μ_2-N1,O1:N2 bridging conformation (Figure 5A). A nearly planar six-membered ring with torsion angles of Cu1–N2–N1–Cu2 and Cu1–N11–N12–Cu2 being 13.16(3) and 12.22(3)° respectively is formed from the double N–N bridges of two opposite pzc co-ligands. This dimeric unit is bridged through a chelating carboxylate

group of pzc into a tetrameric subunit of composition $[Cu_4(pzc)_4]$, which is further bridged by two **L** ligands into double zig-zag chains of composition $[Cu_4(L)_2(pzc)_4(OH_2)_2]_n$ (Figure 5B). The pyridinium units are nearly perpendicular to the 4-carboxylbenzyl motifs with dihedral angles of 65.31(1)/68.06(2)° and pyridinium-CH_2-phenyl angles of 111.51(3)/111.56(4)°, resulting in an intramolecular Cu1–Cu2B distance of 21.22(2) Å (Figure 5A). Six non-coordinating water molecules occupy the intermolecular voids and display extensive intermolecular hydrogen bonding interactions with the carboxylates of **L** resulting in a 3-D supramolecular framework (Figure 5C and SI, Table S1).

Figure 5. (A) Crystal structure of **7** with view on the coordination sphere of the Cd(II) cation with displacement ellipsoids drawn at the 50% probability level. Selected atoms are labelled. Symmetry codes: A = x + 2, y, z, B = x - 2, y, z, B= -x + 1, -y, -z + 1; (B) structural conformation of **L** in **7** with view along the *b* axis; (C) crystal packing with view along the *a* axis, dashed lines indicate intermolecular hydrogen bonding interactions.

Crystal structure of $\{[ZnCl_2(L)_{0.5}]\cdot 1/6H_2O\}_n$ 8

Compound **8** crystallizes in the monoclinic space group *C*2/*c* with the asymmetric unit consisting of one Zn(II) cation, two chloride anions and a half molecule of **L**, with all the atoms in crystallographically independent general positions and one non-coordinating water molecule located on a C_2 rotation axis with SOF of 1/6. In the crystal structure, the Zn(II) cation are each coordinated by one O atom of two bidentate carboxylate groups of **L** and two chloride anions in a tetrahedral geometry (Figure 6A). The carboxylate groups are further coordinated to a symmetry equivalent Zn atom, forming a dimeric unit of composition $[Zn_2(CO_2)_2(Cl)_4]$ with a Zn-Zn distance of 3.693(1) Å. **L** adopts a 'trans' conformation with respect to the relative orientation of the rigid bipyridinium unit, thereby bridging the Zn(II)

cations to form infinite 1-D zig-zag chains (Figure 6B). The pyridinium planes of the rigid bipyridinium unit are co-planar. The dihedral angles between adjacent 4-carboxylbenzyl motifs and the pyridinium rings amount to 83.73(3)° and 84.96(3)°. In the intermolecular crystal packing the chains intersect within the {-2 -2.5 1} plane (Figure 6C) forming 1-D channel pores along the crystallographic *c* axis which are blocked by the coordinating chloride anions (Figure 6D). The smallest inter-chain separation of two metal cations is 5.376(1) Å.

Figure 6. (A) Crystal structure of **8** with view on the coordination sphere of the Cd(II) cation with displacement ellipsoids drawn at the 50% probability level. Selected atoms are labelled. Symmetry codes: A = -x + 1.5, -y - 0.5, -z + 2, B = -x + 0.5, -y + 0.5, -z + 1; (B) structural conformation of **L** in **8** with view along the *c* axis; (C) perspective view towards the {-2 -2.5 1} plane showing the intermolecular intersection of chains; (D) view along the *c* axis showing chloride ions pointing towards pores. Hydrogen atoms and non-coordinating water molecules are removed for the sake of clarity.

Crystal structure of $[Pd(Br)_2(NO_2)_2]\cdot H_2L\cdot 2H_2O$ (9)

Compound **9** crystallizes in the centrosymmetric space group *P*-1 with the asymmetric unit consisting of one half occupied Pd(II) cation located on a center of inversion, one coordinating bromide anion and one coordinating nitrite anion, one non-coordinating water molecule and one half molecule of a non-coordinating protonated ligand H_2**L**, all in crystallographic general positions. In the crystal structure each Pd(II) cation is coordinated by two symmetry related bromide anions and two N-coordinating nitrite anions in a square planar geometry (Figure 7A). The Pd-Br and Pd-N bond distances amount to 2.442(7) Å and 2.184(6) Å respectively. The pyridinium rings of the 4,4'-bipyridinium unit of **L** are co-planar, while the 4-carboxylbenzyl motifs are twisted from the neighboring pyridinium units with a dihedral an-

gle of 69.47(1)°. The two 4-carboxykbenzyl motifs are globally parallel aligned by symmetry resulting in a $O1_{carboxylate}$–$O1A_{carboxylate}$ distance of 18.991(3) Å. Intermolecular hydrogen bonding interactions of C-H···O, O-H···Br and O-H···O can be observed between the non-coordinating water molecule and the bromide and nitrite anions coordinated to the metal center as well as between the carboxyl O atoms and the C-H groups on **L** (SI, Table S2). This hydrogen bonding network results in the formation of a supramolecular coordination polymer with channels along the *b* axis occupied by the $[Pd(Br)_2(NO_2)_2]$ moiety and water molecules.

Figure 7. Crystal structure of **9** with view of the coordination sphere of the Pd(II) cation with displacement ellipsoids drawn at the 50% probability level. Selected atoms are labelled. Symmetry codes: A = -x, -y, -z + 1, B = -x, -y + 1, -z - 1; (B) crystal packing in **9** with view along the *b* axis showing water molecules and the $[Pd(Br)_2(NO_2)_2]$ units occupying the channels. Hydrogen atoms are omitted for the sake of clarity.

Ligand-Metal Coordination Modes

The nature of ligand orientation and metal coordination numbers were found to play a key role in the formation of four different M-L coordination modes in compounds **1**-**9** as shown in the SI, Figure S8: (A) **L** exhibits a μ_4-η^1:η^1:η^1:η^1 coordination mode in **1** and **8** thereby yielding dimeric units of composition $[Cu_2(CO_2)_4(Br)_2]$ in **1** and $[Zn_2(CO_2)_2(Cl)_4]$ in **8**. The metal ions are, however, penta- and tetra-coordinated in **1** and **8** to give rise to a 3-D network and 1-D zig-zag chains respectively; (B) There are two crystallographically distinct metal centers in **2**, **3** and **4**, whereas one is in general position, and the other is located on a crystallographic 3-fold axis. Both metal centers are hexa-coordinated by three water molecules along with three monodentate carboxylates of three ligands. **L** exhibits a μ_2-η^1:η^1 coordination mode thereby resulting in 2-D hexagonal layers, with large honey-comb like hexagonal cavities, held to-

gether by extensive hydrogen bonding interactions; (C and D) **L** displays different conformations and coordination modes in **5** and **6**, namely μ_2-η^2:η^2 for $\mathbf{L}_{cis}$ and μ_2-η^2:η^1 for $\mathbf{L}_{trans}$ with the metal ion being hexa-coordinated to give 1-D chains. A μ_2-η^2:η^2 mode can be found in **7**, similar to that observed for $\mathbf{L}_{cis}$ in **5** and **6**, bridging the dimeric units of composition $[Cu_2(pzc)_2(OH_2)]$ and thereby resulting in the formation of double zig-zag chains of composition $[Cu_4(L)_2(pzc)_4(OH_2)_2]_n$. A further thorough evaluation of various bridging modes of **L** in the CSD database (Version 5.37, November 2015) revealed ten[27, 35, 36, 38, 41] structures with μ_2-η^2:η^2 followed by seven[28, 40, 51] with μ_2-η^1:η^1 coordination mode, three[31, 42, 52] with μ_4-η^1:η^1:η^1:η^1 and two[38, 52] with μ_2-η^2:η^1.

X-ray Powder Diffraction Analysis, IR Spectra and Thermal Properties

Compounds **1-4** displayed stability in the solid state upon exposure to air for weeks. The purity of the samples was confirmed by matching experimental PXRD data with simulated patterns generated from single-crystal diffraction data (SI, Figures S3 and S4). The IR spectra of Ligand **L** and MOFs **1-4** are displayed in the SI, Figure S2. The nitrogen adsorption isotherms collected at 77 K suggest BET surface areas of 9.83, 3.41, 6.45 and 3.00 m^2g^{-1} for compounds **1**, **2**, **3** and **4** respectively (SI, Figure S9). This is not surprising as solvent accessible voids of only 22.1% for **1**, 17.2% for **2**, 17.0% for **3** and 17.1% for **4** can be found.

Thermogravimetric analysis experiments were carried out to evaluate the thermal stabilities of their coordination networks. Upon heating, a two-step weight loss process was observed for **1.** The first experimental weight loss of 8.3% from 30 to 200 °C roughly corresponds to the release of three non-coordinating water molecules as opposed to 25.2% which is expected for seven water molecules as calculated from the single crystal data composition (SI, Figure S10A). This first mass step is accompanied by an endothermic event in the DSC curve. Upon further heating, the anhydrate form starts to decompose at ~220 °C. In accord with the

elemental analysis, it can be assumed that **1** partially dehydrates upon initial exposure to the dynamic nitrogen atmosphere during TGA analysis. This might lead to the removal of four out of seven loosely bound non-coordinating water molecules even before the initiation of thermal analysis. Upon heating compounds **2-4** to 200 °C, one mass step can be observed corresponding to the loss of non-coordinating and coordinating water molecules and each is accompanied by an endothermic event in the DSC curve before decomposition takes place around 250 °C (SI, Figure S10B, C, D). The experimental mass losses of $\Delta m_{exp}(1^{st}$ step) ~17.8, 19.3 and 20.0% are observed for **2**, **3** and **4** respectively which are in good agreement with the expected mass loss of ~19.2% in this temperature range.

Photochromic Behavior

Upon exposure to UV light (365 nm, 100 W, Lamp UVP B-100AP) or sunlight in air at room temperature, a visible color change from ivory to blue is observed within seconds for $(H_2L)_2{\cdot}SO_4{\cdot}HSO_4{\cdot}Br{\cdot}2H_2O$ (Figure 8). Investigations on the reversibility of this process have shown that the blue crystals transform back to the pristine state within a week upon exposure to the regular lab environment, which can be cycled more than ten times. The reversible transformation can be accelerated to time frames of minutes upon heating the crystals to 50 °C in air. This behavior is similar to that observed in the reversible interconversion of viologen dications into monocation viologen radicals.[35, 38, 53-56]

Figure 8. Photochromic effect observed for a single crystalline sample of $(H_2L)_2{\cdot}SO_4{\cdot}HSO_4{\cdot}Br{\cdot}2H_2O$ shown as photographic images before and after UV irradiation.

The orientation of **L** displaying potential inter-ligand electron transfer routes, selected atoms are labelled. Symmetry codes: A = -x + 2, -y + 1, -z - 1, B = -x +1, -y, -z -1.

To obtain deeper insights into structural parameters influencing the photochromic behavior, study was focused on the inter-ligand interactions. (Figure 8). The electron transfer is known to be favorable if the electron donor lies perpendicular and in close proximity above or below the nitrogen atom of the bipyridinium ring. Intermolecular geometries and distances between donor and acceptor units of 70-100° and 3.4-4.0 Å respectively are reported to be suitable for generating radicals.[32, 35, 46, 48, 49] It was found that the shortest intermolecular distances between the pyridinium N atoms and the carboxylate oxygens amount to 3.095Å (N1–O3A) and 3.186Å (N2–O2B) while being approximately perpendicular to each other with angles of 100.4° (O3A–N1–C11) and 103.1° (O2B–N2–C14). It should be noted here that this intermolecular electron donor-acceptor distance is the smallest among the photochromic materials reported with **L**.[38, 41] Similar investigations were carried out on the photochromic behavior of **1-9**, however, to our surprise we found that none of the MOFs exhibited a similar color change to the one observed for **L**. Interestingly, the isostructural framework of **5** and **6** is reported to be photochromic.[38] This behavior is reported to originate from the sandwich-type D···A···D stacking between the bdc co-ligand and bipyridinium units with their π planes approximately parallel to each other. The pyridinium N to carboxylate O geometries of 3.57 Å and 91.36°, are reported, [32,35,49,51,52] however, a detailed structural analysis of the isostructural compounds **5** and **6** reveals the corresponding distances and angle of 3.11/3.08 Å and 96.36/104.71°. Based on this observation, it can be speculated that only the deviation of 5.00/13.35° for e^- donor-acceptor angle, with respect to the reported isostructural material, could be the reason why photochromic behavior could not be observed in **5** and **6**. In general, investigations showed a deviation from perpendicularity between the electron donor and acceptor moieties for **1-9** along with large separations between the two, rendering the electron transfer process unfavorable.[38]

A thorough structural analysis was performed to determine if any intra- and/or intermolecular structural parameters of **L**, with its electron acceptor (pyridinium-N) and electron donor (carboxyl-O) units, result in the occurrence of photochromic behavior. Selected intra- and intermolecular geometries/distances are given in Figure 9 and Table 2. We conclude that no intermolecular correlation could be found, revealing that, if observed, the photochromic behavior can be traced back only to favorable intermolecular distances and angles between the electron donor and electron acceptor species. Note that some compounds show favorable intermolecular parameters, but apparently they were not tested for their potential photochromism.

Figure 9. Structural analysis of **L**. α denotes the dihedral angle between the pyridinium rings; β1 (β2) represent the dihedrals between the pyridinium ring and the adjacent 4-carboxylbenzyl unit; Θ denotes the dihedral angle between the two 4-carboxylbenzyl units; and ϕ1 (ϕ2) are the bond angles as labelled.

Table 2. Systematic overview of important intra- and intermolecular structural parameters of **L** in the compounds studied and those reported in literature. Refer to the labelling scheme in Figure 8 and 9.

Compound	α [deg]	β1 (β2) [deg]	Θ [deg]	ϕ1 (ϕ2) [deg]	D–A (∠O–N–C)* [Å, deg]	Photochromic behavior	Reference
$(H_2\mathbf{L})_2{\cdot}SO_4{\cdot}HSO_4{\cdot}Br{\cdot}2H_2O$	3.01	72.96 (73.32)	1.13	110.68 (110.61)	3.095 (100.4), 3.186 (103.1)	yes	this work
$\{[CuBr(\mathbf{L})]{\cdot}(OH){\cdot}7H_2O\}_n$ (**1**)	29.67	84.40	60.62	107.75	>4.0	no	this work
$\{[Mn_4(\mathbf{L})_6(OH_2)_{12}]{\cdot}2Br{\cdot}3(bdc){\cdot}33H_2O\}_n$ (**2**)	13.47	77.51 (72.72)	5.48	110.73 (111.47)	>4.0	no	this work
$\{[Co_4(\mathbf{L})_6(OH_2)_{12}]{\cdot}2Br{\cdot}3(bdc){\cdot}33H_2O\}_n$ (**3**)	5.98	72.83 (76.45)	9.36	111.04 (111.18)	>4.0	no	this work
$\{[Ni_4(\mathbf{L})_6(OH_2)_{12}]{\cdot}2Br{\cdot}3(bdc){\cdot}33H_2O\}_n$ (**4**)	13.11	72.42 (77.61)	5.37	111.72 (111.24)	>4.0	no	this work
$\{[Cd(bdc)(\mathbf{L})_{1.5}]{\cdot}9H_2O\}_n$ (**5**)	31.10 0	73.93 (86.85) 83.98	10.19 0	108.74 (110.97) 110.53	3.114 (96.3)	no	this work
$\{[Zn(bdc)(\mathbf{L})_{1.5}]{\cdot}9H_2O\}_n$ (**6**)	26.98 0	76.10 (83.38) 87.80	10.88 0	110.88 (110.00) 110.83	3.080 (104.7), 3.894 (106.3), 3.974 (104.7)	no	this work
$\{[Cu_2(3\text{-}pzc)_2(\mathbf{L})(OH_2)]{\cdot}5H_2O\}_n$ (**7**)	52.14	68.06 (65.30)	31.41	111.53	3.079 (72.3), 3.224 (73.6), 3.282 (112.6), 3.403 (111.9)	no	this work
$\{[ZnCl_2(\mathbf{L})_{0.5}]{\cdot}0.33H_2O\}_n$ (**8**)	0	69.15	0	110.35	>4.0	no	this work
$[Pd(H\mathbf{L})(Br)_2(NO_2)_2(H_2O)_2]$ (**9**)	0	69.47	0	110.58	3.829 (119.1)	no	this work
$[Co_3(\mathbf{L})_4(N_3)_2(H_2O)_2]{\cdot}4NO_3$	0	75.38	0	110.81	3.523 (89.1), 3.843 (113.6)	no	[52]
$\{[CdBr_2(\mathbf{L})]{\cdot}4H_2O\}_n$	13.46	83.94 (84.20)	21.80	112.52 (113.54)	3.549 (73.8), 3.643 (96.2)	yes	[35]
$\{[Zn_2(\mathbf{L})_3(bdc)_2]{\cdot}4H_2O\}_n$	23.15	81.84	8.06	107.18 (110.50)	3.410 (108.0)	no	[57]
$\{[Cd(\mathbf{L})_2]{\cdot}2ClO_4{\cdot}7H_2O\}_n$	35.86	74.75	12.30	110.17	3.930 (113.2), 3.911 (90.6)	no	[36]
$\{[Cd(Cl)_2(\mathbf{L})]{\cdot}4.5H_2O\}_n$	15.72	84.59 (88.43)	17.71	111.46 (112.25)	3.371 (80.5), 3.803 (99.4)	yes	[36]
$\{[Cd(SCN)_2(\mathbf{L})]\}_n$	14.98	87.73	9.57	112.28 (111.66)	3.274 (83.6), 3.467 (103.3), 3.906 (103.3)	yes	[36]

$\{[Cd(N_3)_2(\mathbf{L})]\cdot 3H_2O\}_n$	11.96	89.46 (88.27)	9.34	111.51 (112.75)	3.474 (76.4), 3.499 (102.4), 3.937 (96.2)	yes	36
$\{[Cd(I)_2(\mathbf{L})]\}_n$	6.29	88.22 (87.05)	6.74	112.06 (113.12)	3.391 (83.4), 3.609 (100.4), 3.880 (105.5)	yes	36
$[(H\mathbf{L})(BF_4)]\cdot 2H_2O$	62.09	72.97 (71.78)	74.45	112.88 (111.92)	3.303 (107.3), 3.890 (109.2), 3.872 (117.1)	yes	37
$[(H\mathbf{L})(BF_4)]\cdot 3H_2O$	23.59	84.16 (72.51)	85.64	110.92 (110.98)	3.147 (98.8), 3.982 (80.9)	yes	37
$\{[Eu(ba)(\mathbf{L})_{1.5}(OH_2)]_2\cdot NO_3\cdot 5H_2O\}_n$	0	89.48	0	111.34	3.782 (72.9), 3.808 (121.8)	yes	41
$\{(\mathbf{L})_3[Mn_2(OH_2)_6](OH)_4\cdot 15H_2O\}_n$	0	75.27	0	112.77	>4.0	no	40
$\{(\mathbf{L})_3[Co_2(OH_2)_6](OH)_4\cdot 15H_2O\}_n$	0	76	0	110.76	>4.0	no	40
$\{(\mathbf{L})_3[Ni_2(OH_2)_6](OH)_4\cdot 15H_2O\}_n$	0	75.89	0	110.80	>4.0	no	40
$\mathbf{L}\cdot 5H_2O$	7.425	88.89	51.68	111.53	3.376 (102.9)	yes	58
$\{[Cd(bdc)(\mathbf{L})_{1.5}]\cdot 10H_2O\}_n$	16.99	84.43 (78.66)	10.41	111.58	3.569 (91.4)	yes	38
$\{[Cu_2(\mathbf{L})_2(NO_3)_2]\cdot 0.5Cl\cdot 0.5(OH)\cdot NO_3\cdot 8H_2O\}_n$	28.84	83.61	63.4	112.19	3.752 (78.6)	no	31
$\{[Dy(ox)(\mathbf{L})(OH_2)](OH)\cdot 13H_2O\}_n$	17.86	89.61 (86.04)	78.83	111.59 (107.79)	3.945(106.0)	no	27
$\{[Ni(H_2O)_4(\mathbf{L})(pta)]\cdot 9H_2O\}_n$	4.90	79.67 (89.95)	44.14	108.26 (109.74)	3.206 (97.4), 3.589 (79.8), 3.762 (98.2)	no	42
$\{[Zn_4(\mathbf{L})_6(H_2O)_{12}](OH)_8\cdot 9H_2O\}_{2n}$	7.53	74 (76.99)	4.72	109.90 (110.03)	3.809 (62.9)	no	51
$[\{Mn(\mathbf{L})_{1.5}(H_2O)_3\}\cdot SO_4\cdot 10.5H_2O]_n$	0	74.83	0	111.28	>4.0	no	28
$[\{Mn_4(\mathbf{L})_6(H_2O)_{12}\}\cdot(bdc)_3\cdot(OH)_2\cdot 30H_2O]_n$	6.41	73.23 (76.45)	9.38	110.79 (110.93)	3.728 (66.7), 3.803 (121.2)	no	28
$[\{Eu_4(\mathbf{L})_6(H_2O)_9(SO_4)_3\}\cdot(OH)_6\cdot 51.5H_2O]_n$	4.38	78.16 (75.53)	4.57	109.33 (113.08)	3.758 (71.0)	no	28

bdc = 1,4-benzenedicarboxylate, pzc = 3-pyrazole carboxylate, ba = benzoic acid, ox = oxalic acid, pta = potassium hydrogen phthalate;
*$O_{carboxyl}$ = electron acceptor, $N_{pyridinium}$ = electron acceptor, C = carbon atom in 4 position of the pyridinium unit.

Conclusion

A series of nine new ZW MOFs based on the viologen ligand 1,1'-bis(4-carboxybenzyl)-4,4'-bipyridinium dibromide (H_2**L**Br_2) and various anionic counterions have been successfully synthesized and crystallized under mild conditions exhibit various versatile coordination features. Thorough structural investigations revealed that different anionic counterions have a significant effect on the structures of the resulting MOFs. **1** exhibits a 3-D polymeric framework with copper paddlewheel dimeric units as node and counterbalancing bromide anions in the axial positions of the paddlewheel. The isostructural compounds **2**, **3** and **4** are composed of a 2-D network with the non-coordinating co-ligand bdc incorporated into the pores, whereas **5** and **6** with metal-coordinated bdc display 1-D chains as structural motif. A supramolecular 3-D framework consisting of double zig-zag chains stabilized by intermolecular hydrogen bonding interactions is found for **7**, whereas **8** exhibits a supramolecular 3-D framework formed by intersecting zig-zag chains. Interestingly, upon UV light irradiation, photochromic behavior was observed for the crystallized ligand of composition $(H_2L)_2 \cdot SO_4 \cdot HSO_4 \cdot Br \cdot 2H_2O$, which was found to originate from the formation of viologen radicals. A systematic literature analysis of important intra- and intermolecular structural parameters of the ligand have revealed that intermolecular geometries and distances between the electron donor and acceptor units are the only dominating factor enabling photochromic properties. However, if this is a general trend must be investigated in more detail through additional systematic investigations on the structure-property relationships of similar ZW materials.

Acknowledgment

We gratefully acknowledge Clarkson University for generous start-up funding and the Donors of the American Chemical Society Petroleum Research Fund (56295-DNI10) for support of this research.

Supporting information available

NMR data of H_2LBr_2; IR data of H_2LBr_2 and **1**-**4**; PXRD data of **1**-**4**; temperature ellipsoid plot of **2**, **4** and **6**; characteristic bond distances and angles for hydrogen bonding interactions of **2**-**4** and **7**; coordination modes exhibited by L in **2**-**9**; comments on B-alerts of checkcif reports; N_2 adsorption isotherms at 77 K of **1**-**4**; TGA and DSC curves of **1**-**4**.

References

1. J. S. Seo, D. Whang, H. Lee, S. I. Jun, J. Oh, Y. J. Jeon and K. Kim, *Nature*, 2000, **404**, 982.
2. Y.-Z. Chen, Y.-X. Zhou, H. Wang, J. Lu, T. Uchida, Q. Xu, S.-H. Yu and H.-L. Jiang, *ACS Catal.*, 2015, **5**, 2062.
3. H.-Q. Xu, J. Hu, D. Wang, Z. Li, Q. Zhang, Y. Luo, S.-H. Yu and H.-L. Jiang, *J. Am. Chem. Soc.*, 2015, **137**, 13440.
4. S. Saha, G. Das, J. Thote and R. Banerjee, *J. Am. Chem. Soc.*, 2014, **136**, 14845.
5. H. J. Choi and M. P. Suh, *J. Am. Chem. Soc.*, 2004, **126**, 15844.
6. E. Y. Lee and M. P. Suh, *Angew. Chem. Int. Ed.*, 2004, **43**, 2798.
7. J.-R. Li, J. Sculley and H.-C. Zhou, *Chem. Rev.*, 2011, **112**, 869.
8. D. Britt, H. Furukawa, B. Wang, T. G. Glover and O. M. Yaghi, *Proc. Natl. Acad. Sci.*, 2009, **106**, 20637.
9. W.-W. He, S.-L. Li, W.-L. Li, J.-S. Li, G.-S. Yang, S.-R. Zhang, Y.-Q. Lan, P. Shen and Z.-M. Su, *J. Mater. Chem. A*, 2013, **1**, 11111.
10. Y. He, W. Zhou, G. Qian and B. Chen, *Chem. Soc. Rev.*, 2014, **43**, 5657.
11. M. B. Lalonde, R. B. Getman, J. Y. Lee, J. M. Roberts, A. A. Sarjeant, K. A. Scheidt, P. A. Georgiev, J. P. Embs, J. Eckert, O. K. Farha, R. Q. Snurr and J. T. Hupp, *CrystEngComm*, 2013, **15**, 9408.
12. L. Li, S. Tang, C. Wang, X. Lv, M. Jiang, H. Wu and X. Zhao, *Chem. Commun.*, 2014, **50**, 2304.
13. M. P. Suh, H. J. Park, T. K. Prasad and D.-W. Lim, *Chem. Rev.*, 2011, **112**, 782.
14. T. B. Faust and D. M. D'Alessandro, *RSC Advances*, 2014, **4**, 17498.

15. H. Li, X. Feng, Y. Guo, D. Chen, R. Li, X. Ren, X. Jiang, Y. Dong and B. Wang, *Sci. Rep.*, 2014, **4**, 4366.
16. A. Schneemann, V. Bon, I. Schwedler, I. Senkovska, S. Kaskel and R. A. Fischer, *Chem. Soc. Rev.*, 2014, **43**, 6062.
17. C. K. Brozek and M. Dinca, *Chem. Soc. Rev.*, 2014, **43**, 5456.
18. J. D. Evans, C. J. Sumby and C. J. Doonan, *Chem. Soc. Rev.*, 2014, **43**, 5933.
19. X. Zhao, X. Bu, T. Wu, S.-T. Zheng, L. Wang and P. Feng, *Nat. Commun.*, 2013, **4**. 2344.
20. P. Ramaswamy, N. E. Wong and G. K. H. Shimizu, *Chem. Soc. Rev.*, 2014, **43**, 5913.
21. T. Zhang and W. Lin, *Chem. Soc. Rev.*, 2014, **43**, 5982.
22. J. R. Long and O. M. Yaghi, *Chem. Soc. Rev.*, 2009, **38**, 1201, all articles of this special issue.
23. H.-C. Zhou, J. R. Long and O. M. Yaghi, *Chem. Rev.*, 2012, **112**, 673, all articles of this special issue.
24. V. Stavila, A. A. Talin and M. D. Allendorf, *Chem. Soc. Rev.*, 2014, **43**, 5994.
25. W.-Y. Gao, M. Chrzanowski and S. Ma, *Chem. Soc. Rev.*, 2014, **43**, 5841.
26. Z. Hu, B. J. Deibert and J. Li, *Chem. Soc. Rev.*, 2014, **43**, 5815.
27. J.-K. Sun, M. Ji, C. Chen, W.-G. Wang, P. Wang, R.-P. Chen and J. Zhang, *Chem. Commun.*, 2013, **49**, 1624.
28. J.-K. Sun, Q.-X. Yao, Y.-Y. Tian, L. Wu, G.-S. Zhu, R.-P. Chen and J. Zhang, *Chem. Eur. J.*, 2012, **18**, 1924.
29. X. Li, X. Guo, X. Weng and S. Lin, *CrystEngComm*, 2012, **14**, 1412.
30. X.-B. Li, J.-Y. Zhang, Y.-Q. Wang, Y. Song and E.-Q. Gao, *Chem. Eur. J.*, 2011, **17**, 13883.
31. H.-X. Zhang, Q.-X. Yao, X.-H. Jin, Z.-F. Ju and J. Zhang, *CrystEngComm*, 2009, **11**, 1807.
32. Y. Ma, X.-B. Li, X.-C. Yi, Q.-X. Jia, E.-Q. Gao and C.-M. Liu, *Inorg. Chem.*, 2010, **49**, 8092.
33. Y.-Q. Wang, A.-L. Cheng, X. Wang and E.-Q. Gao, *RSC Advances*, 2012, **2**, 10352.
34. Y.-Q. Wang, Q. Sun, Q. Yue, A.-L. Cheng, Y. Song and E.-Q. Gao, *Dalton Trans.*, 2011, **40**, 10966.
35. J.-K. Sun, P. Wang, C. Chen, X.-J. Zhou, L.-M. Wu, Y.-F. Zhang and J. Zhang, *Dalton Trans.*, 2012, **41**, 13441.

36. J.-K. Sun, P. Wang, Q.-X. Yao, Y.-J. Chen, Z.-H. Li, Y.-F. Zhang, L.-M. Wu and J. Zhang, *J. Mater. Chem.*, 2012, **22**, 12212.
37. J.-K. Sun, X.-H. Jin, L.-X. Cai and J. Zhang, *J. Mater. Chem.*, 2011, **21**, 17667.
38. Q.-X. Yao, Z.-F. Ju, X.-H. Jin and J. Zhang, *Inorg. Chem.*, 2009, **48**, 1266.
39. D. Aulakh, J. R. Varghese and M. Wriedt, *Inorg. Chem.*, 2015, **54**, 1756.
40. Y.-Q. Sun, J. Zhang, Z.-F. Ju and G.-Y. Yang, *Cryst. Growth Des.*, 2005, **5**, 1939.
41. J.-K. Sun, L.-X. Cai, Y.-J. Chen, Z.-H. Li and J. Zhang, *Chem. Commun.*, 2011, **47**, 6870.
42. Q.-X. Yao, L. Pan, X.-H. Jin, J. Li, Z.-F. Ju and J. Zhang, *Chem. Eur. J.*, 2009, **15**, 11890.
43. Q.-X. Yao, X.-H. Jin, Z.-F. Ju, H.-X. Zhang and J. Zhang, *CrystEngComm*, 2009, **11**, 1502.
44. *SAINT and APEX 2 Software for CCD Diffractometers*, Bruker AXS Inc., Madison, Wisconsin, USA, 2014.
45. G. M. Sheldrick, *SADABS, version 2014/4*, University of Göttingen, Germany, 2014.
46. G. M. Sheldrick, *Acta Crystallogr., Sect. A: Found. Crystallogr.,* 2008, **A64**, 112.
47. G. M. Sheldrick, *Acta Crystallogr.*, 2015, **A71**, 3.
48. G. M. Sheldrick, *Acta Crystallogr.*, 2015, **C71**, 3.
49. *OLEX2: a complete structure solution, refinement and analysis program*, O. V. Dolomanov, L. J. Bourhis, R. J. Gildea, J. A. K. Howard and H. Puschmann, *J. Appl. Cryst,* 2009, **42**, 339.
50. C. F. Macrae, I. J. Bruno, J. A. Chisholm, P. R. Edgington, P. McCabe, E. Pidcock, L. Rodriguez-Monge, R. Taylor, J. van de Streek and P. A. Wood, *J. Appl. Crystallogr.*, 2008, **41**, 466.
51. J.-X. Chen, W.-E. Lin, C.-Q. Zhou, L. F. Yau, J.-R. Wang, B. Wang, W.-H. Chen and Z.-H. Jiang, *Inorg. Chim. Acta*, 2011, **376**, 389.
52. Q.-H. Tan, Y.-Q. Wang, H.-T. Liu and Z.-L. Liu, *Inorg. Chem. Commun.*, 2015, **58**, 67.
53. K. Fu, C.-X. Ren, C. Chen, L.-X. Cai, B. Tan and J. Zhang, *CrystEngComm*, 2014, **16**, 5134.

54. X.-H. Jin, J.-K. Sun, X.-M. Xu, Z.-H. Li and J. Zhang, *Chem. Commun.*, 2010, **46**, 4695.

55. Y. Tan, H. Chen, J. Zhang, S. Liao, J. Dai and Z. Fu, *CrystEngComm*, 2012, **14**, 5137.

56. Y. Zeng, S. Liao, J. Dai and Z. Fu, *Chem. Commun.*, 2012, **48**, 11641.

57. J.-X. Chen, W.-E. Lin, M. Chen, F.-C. Que, L. Tao, X.-L. Cen, Y.-M. Zhou and W.-H. Chen, *Inorg. Chim. Acta*, 2014, **409**, 195.

58. Q.-X. Yao, W.-M. Xuan, H. Zhang, C.-Y. Tu and J. Zhang, *Chem. Commun.*, 2009, 59.

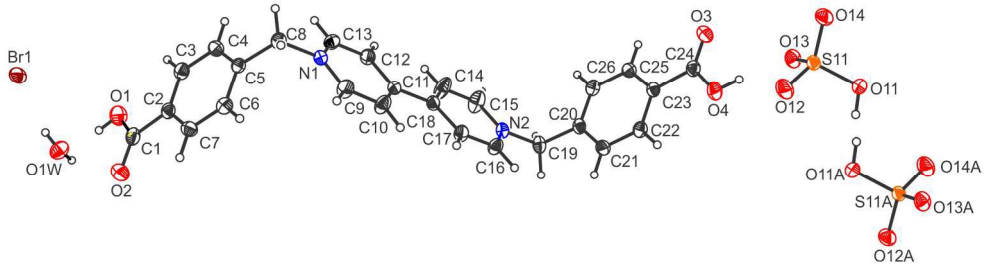

Fig 1
1417x393mm (55 x 55 DPI)

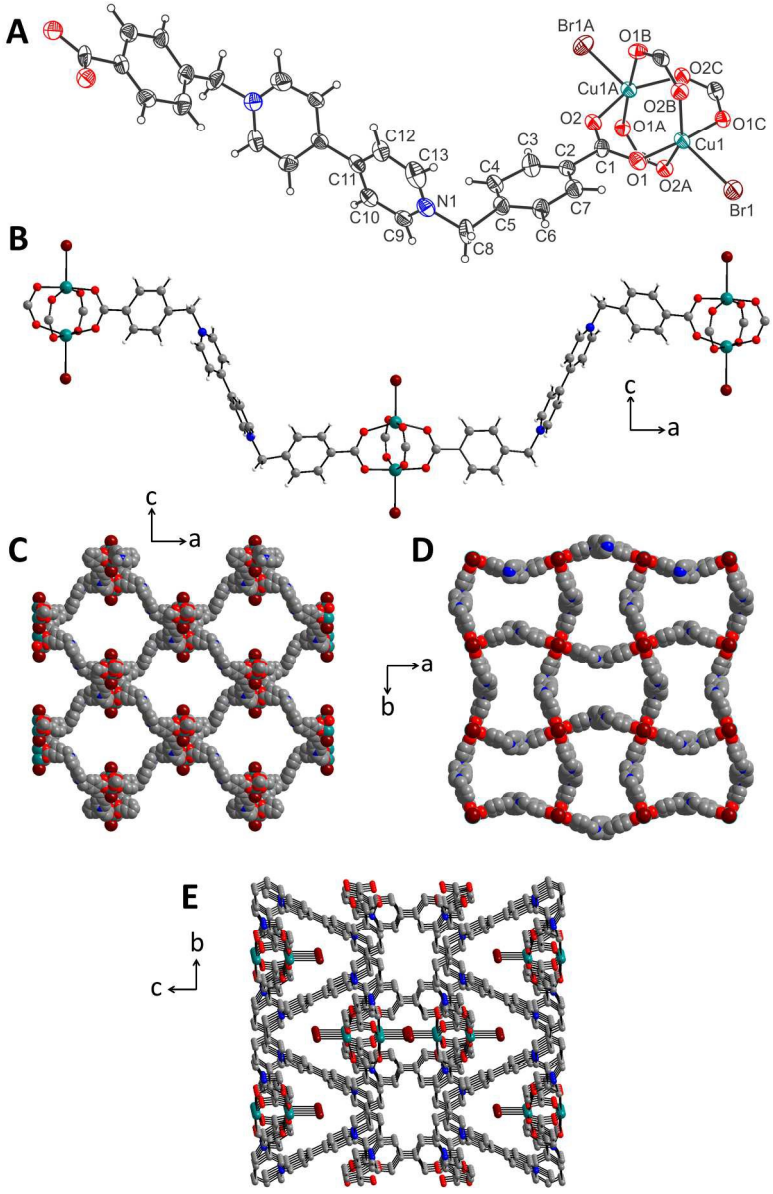

Fig 2
870x1342mm (55 x 55 DPI)

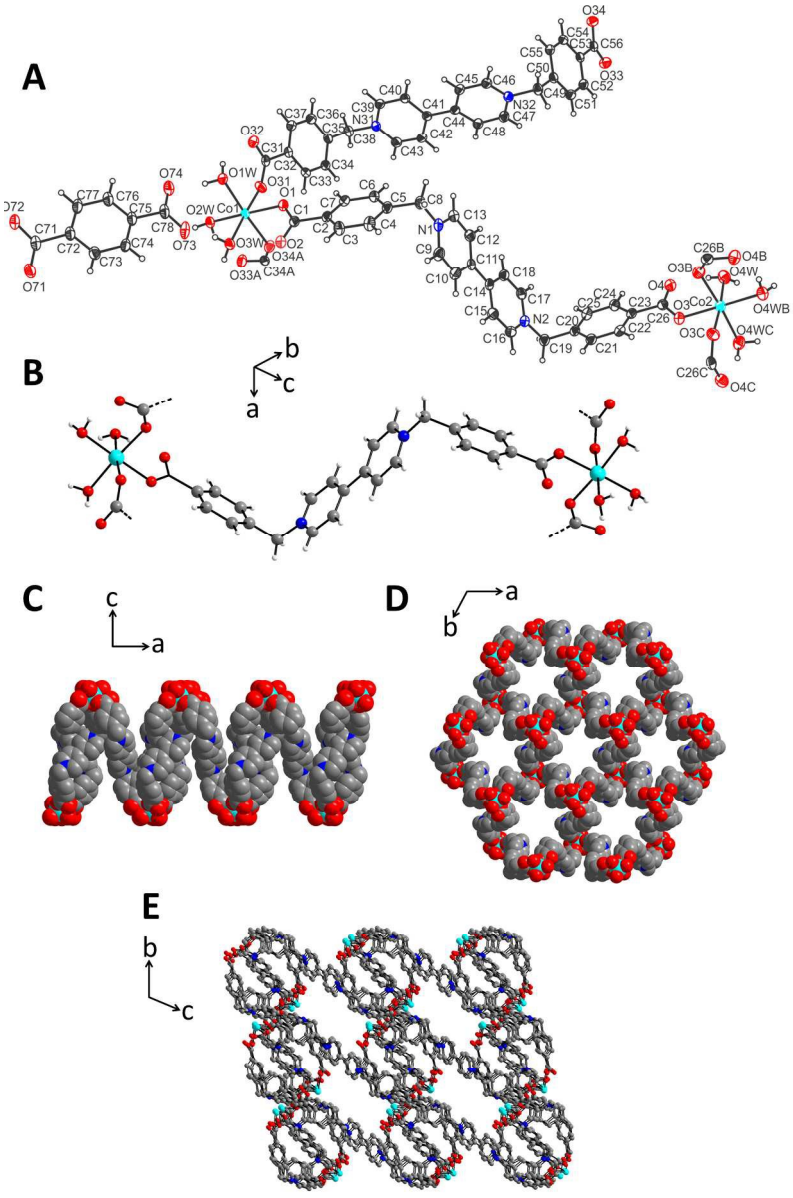

Fig 3
843x1265mm (55 x 55 DPI)

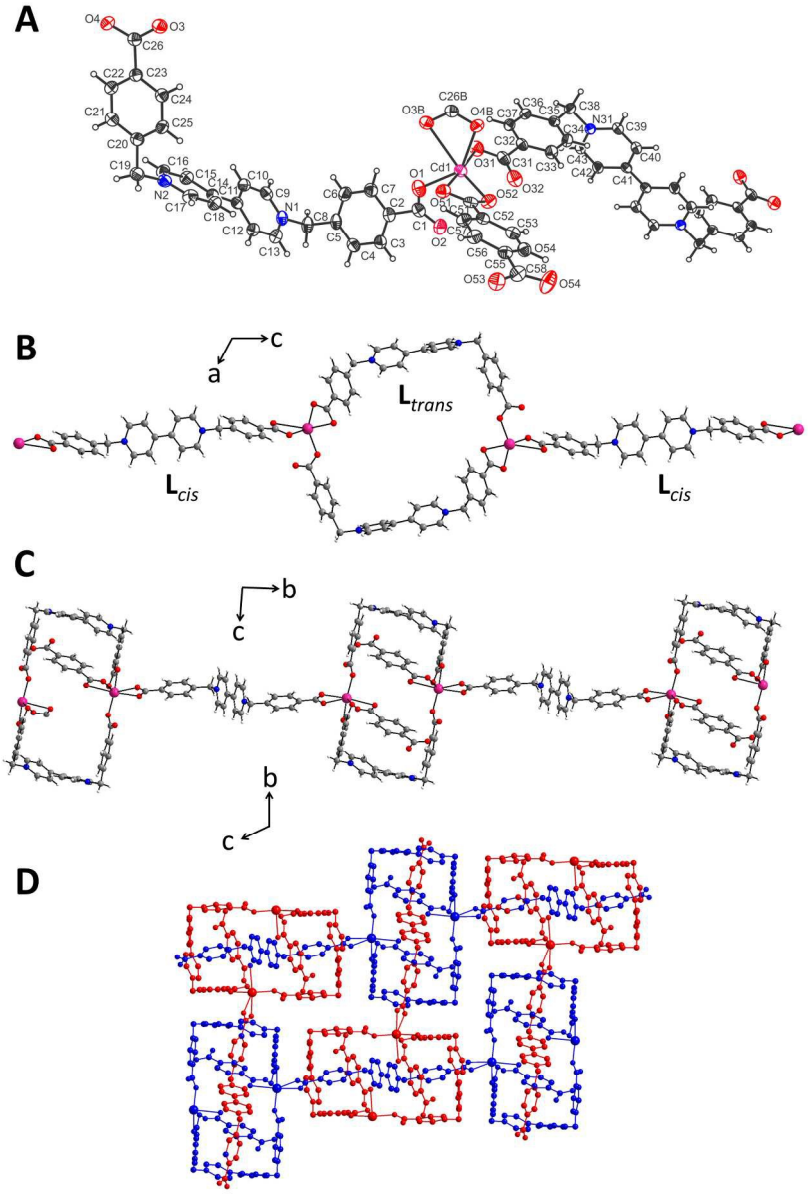

Fig 4
878x1260mm (55 x 55 DPI)

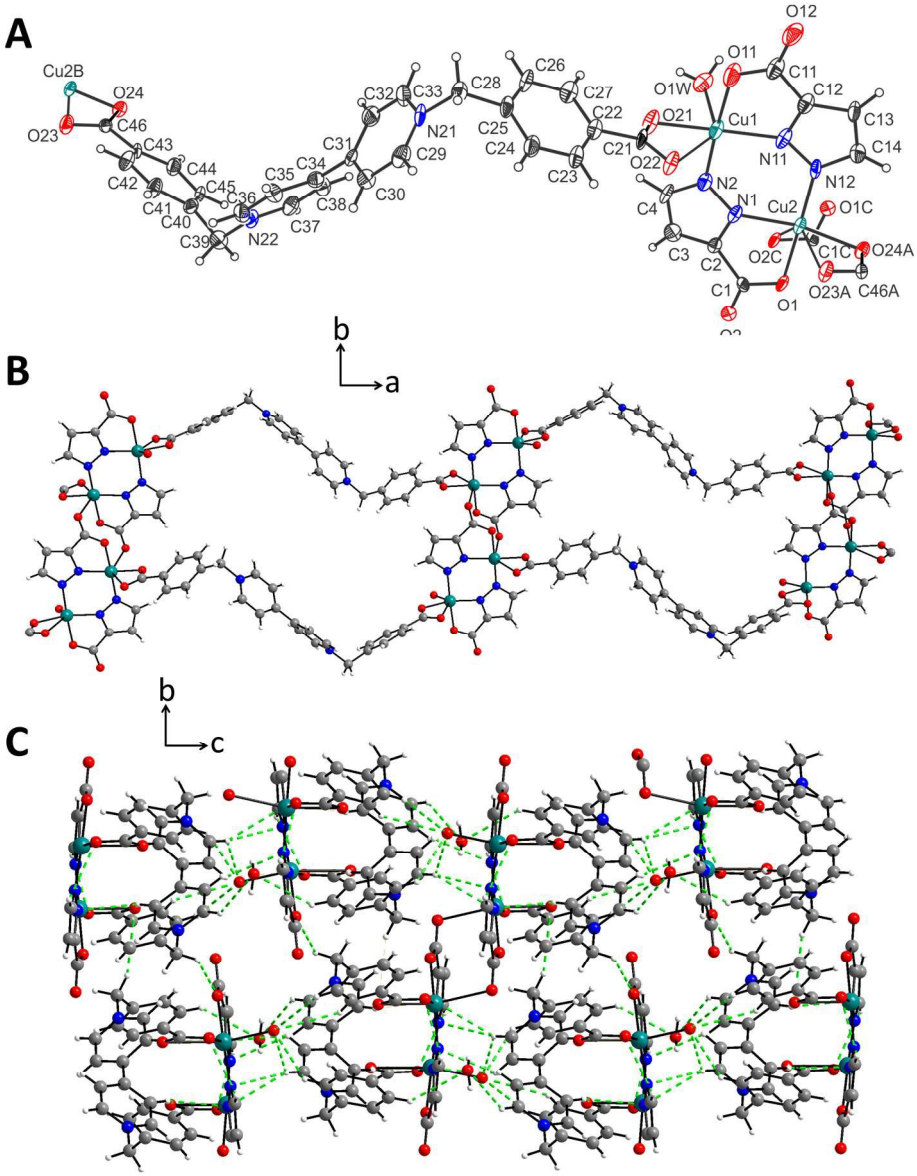

Fig 5
849x1107mm (55 x 55 DPI)

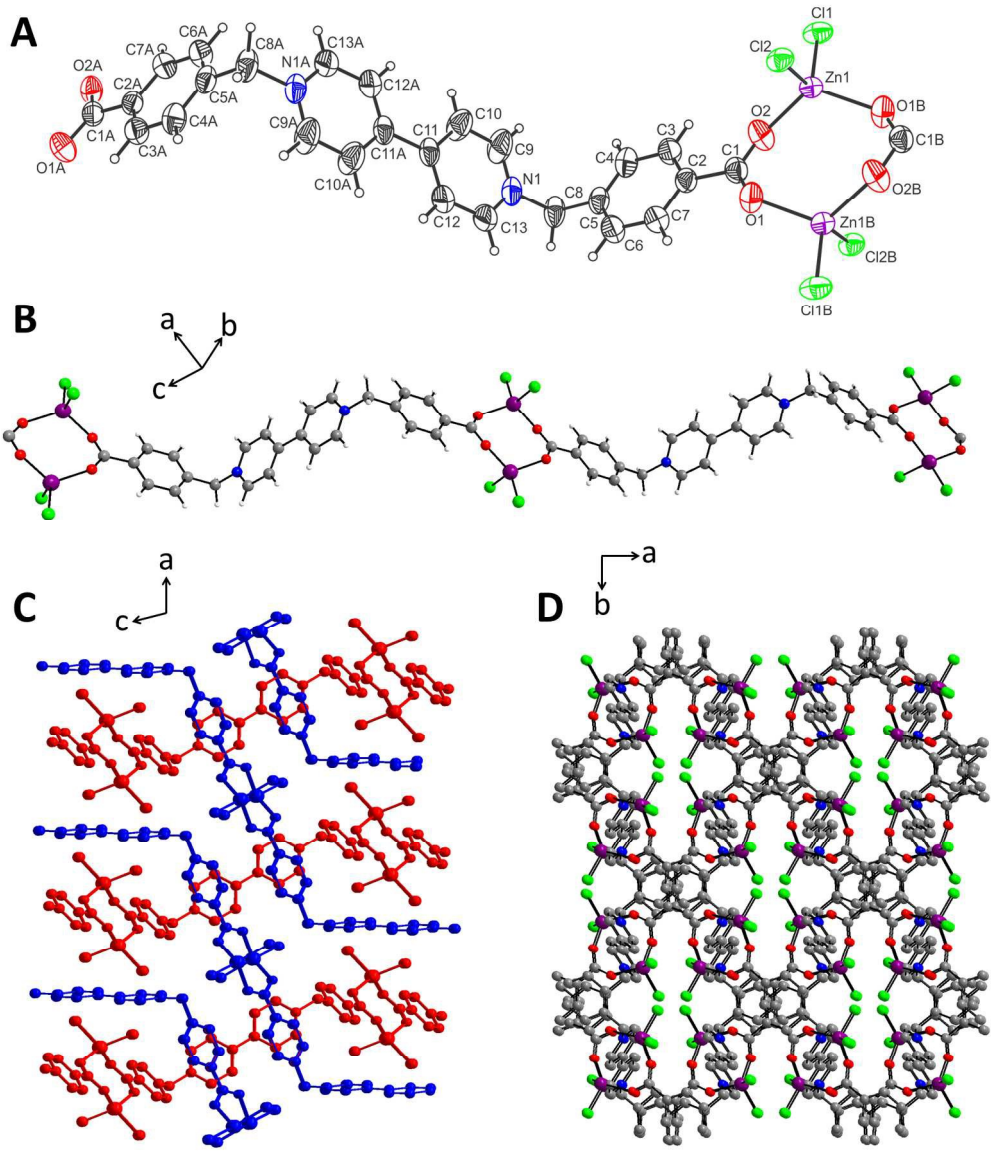

Fig 6
939x1106mm (55 x 55 DPI)

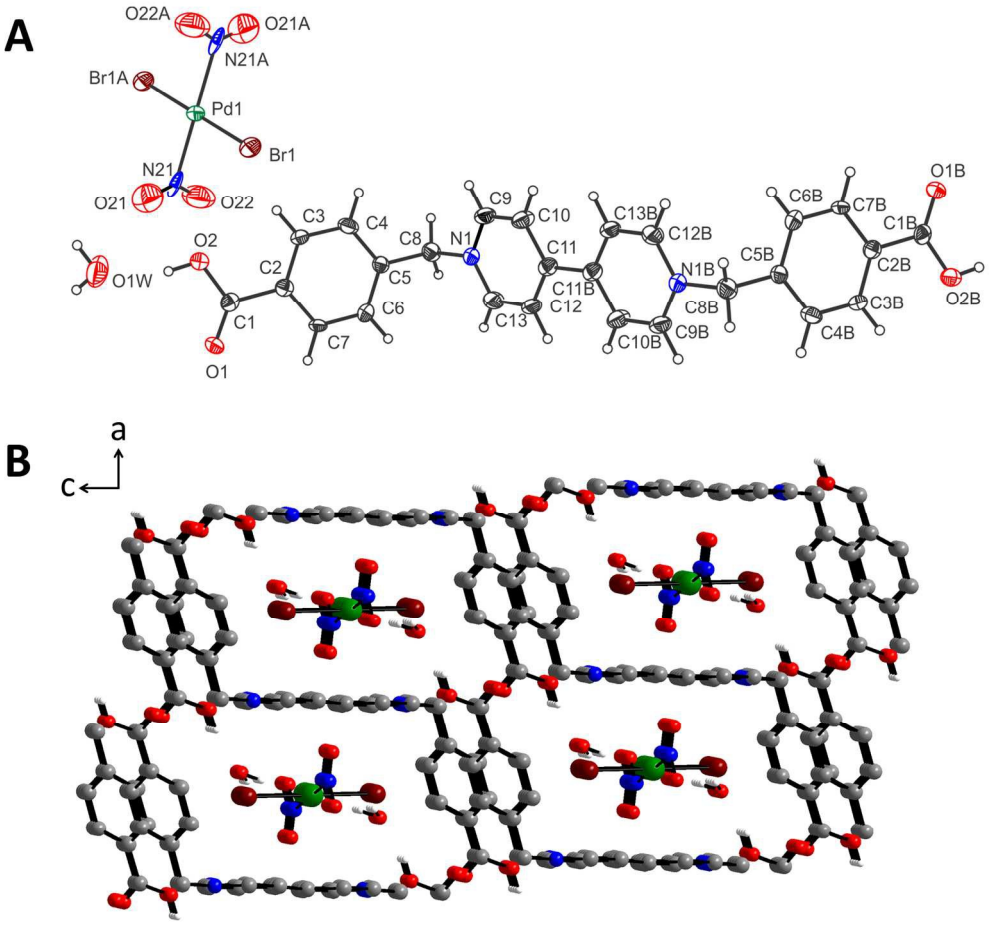

Fig 7
857x810mm (55 x 55 DPI)

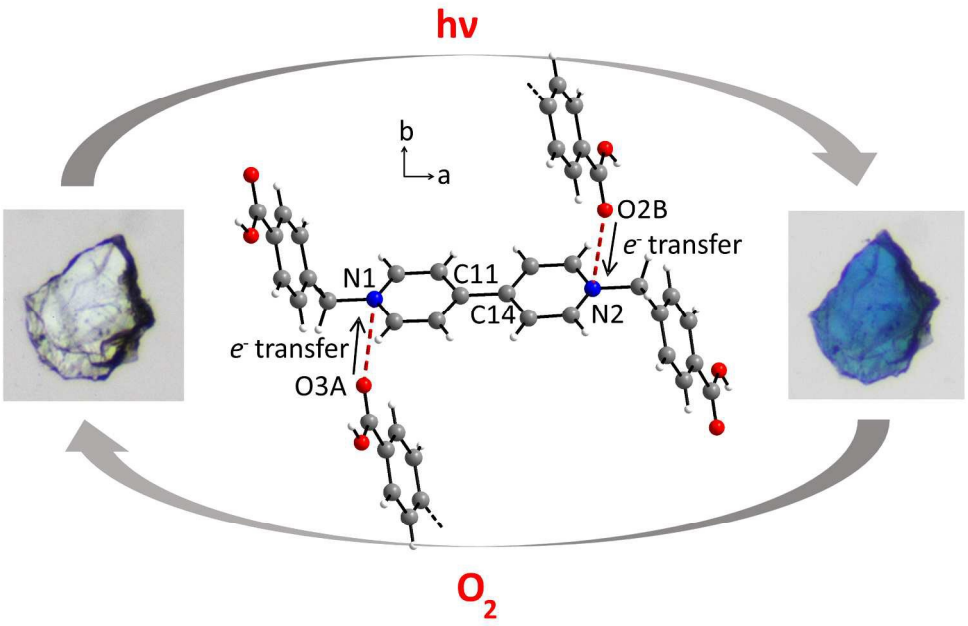

Fig 8
1299x826mm (55 x 55 DPI)

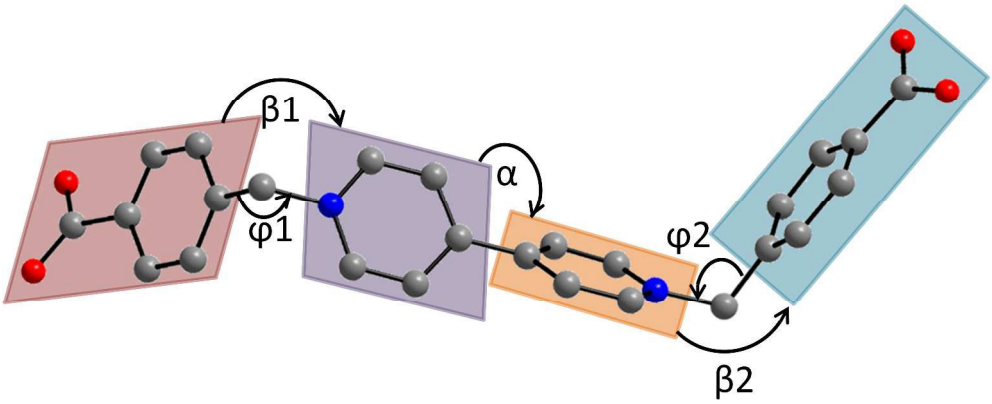

Fig 9
1306x522mm (96 x 96 DPI)

Graphical Abstract

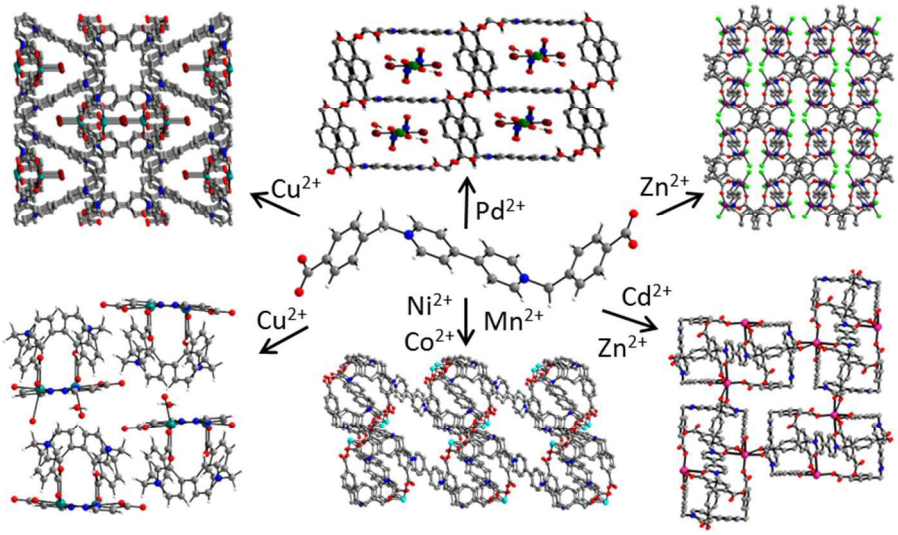

A viologen based ligand has been explored as a functional building block to synthesize a series of nine new zwitterionic metal-organic frameworks with this contribution reporting on their structural, thermal and photochromic properties.